THE JOURNAL OF BIOLOGICAL CHEMISTRY VOL. 282, NO. 19, pp. 14525–14535, May 11, 2007
Printed in the U.S.A.

Solution NMR Structure of the Barrier-to-Autointegration Factor-Emerin Complex*

Received for publication, January 19, 2007, and in revised form, February 27, 2007 Published, JBC Papers in Press, March 13, 2007, DOI 10.1074/jbc.M700576200

Mengli Cai[‡], Ying Huang[§], Jeong-Yong Suh[‡], John M. Louis[‡], Rodolfo Ghirlando[§], Robert Craigie[§], and G. Marius Clore[‡1]

From the Laboratories of [‡]Chemical Physics and [§]Molecular Biology, NIDDK, National Institutes of Health, Bethesda, Maryland 20892-0520

The barrier-to-autointegration factor BAF binds to the LEM domain (Em^{LEM}) of the nuclear envelope protein emerin and plays an essential role in the nuclear architecture of metazoan cells. In addition, the BAF_2 dimer bridges and compacts double-stranded DNA nonspecifically via two symmetry-related DNA binding sites. In this article we present biophysical and structural studies on a complex of BAF_2 and Em^{LEM}. Light scattering, analytical ultracentrifugation, and NMR indicate a stoichiometry of one molecule of Em^{LEM} bound per BAF_2 dimer. The equilibrium dissociation constant (K_d) for the interaction of the BAF_2 dimer and Em^{LEM}, determined by isothermal titration calorimetry, is 0.59 ± 0.03 μM. *Z*-exchange spectroscopy between corresponding cross-peaks of the magnetically non-equivalent subunits of the BAF_2 dimer in the complex yields a dissociation rate constant of 78 ± 2 s^{-1}. The solution NMR structure of the BAF_2-Em^{LEM} complex reveals that the LEM and DNA binding sites on BAF_2 are non-overlapping and that both subunits of the BAF_2 dimer contribute approximately equally to the Em^{LEM} binding site. The relevance of the implications of the structural and biophysical data on the complex in the context of the interaction between the BAF_2 dimer and Em^{LEM} at the nuclear envelope is discussed.

The barrier to autointegration factor (BAF)[2] (1) and the inner nuclear envelope LEM-domain protein emerin (2) are highly conserved cellular proteins throughout the metazoan kingdom that play an important role in nuclear architecture (3). BAF is an all-helical obligate dimer (4) that possesses two symmetry related DNA binding sites that permit BAF to bridge DNA chains and thereby compact DNA (5). Emerin is a member of the LEM (LAP2, Emerin, MAN1) family of nuclear proteins, and its loss is associated with the X-linked recessive form of Emery-Dreifuss muscular dystrophy (6). Emerin is a multidomain protein comprising an N-terminal globular LEM domain (Em^{LEM}) of ~50 residues (7), followed by two polyserine segments separated by a hydrophobic nuclear localization signal, and a C-terminal transmembrane region. Em^{LEM} comprises three helices (8) and is very similar in structure to the LEM domain of the related nuclear envelope protein LAP2 (9). BAF binds to Em^{LEM} (as well as to the LEM domain of LAP2; Ref. 9) and is required for assembly of emerin at the nuclear envelope (10). BAF prevents autointegration of Moloney murine leukemia virus pre-integration complexes *in vitro* (1), and BAF and emerin have been reported to promote engagement of the HIV-1 pre-integration complex with chromatin prior to integration (11). To further our understanding of the interaction between BAF and the LEM domain of emerin we have characterized the stoichiometry of the complex by NMR, light scattering, and analytical ultracentrifugation; determined the equilibrium constant by isothermal titration calorimetry (ITC) and the dissociation rate constant by *z*-exchange spectroscopy; and solved the three-dimensional structure of the complex in solution by multidimensional heteronuclear NMR spectroscopy.

EXPERIMENTAL PROCEDURES

Protein Expression and Purification—The LEM domain (residues 1–47) of human emerin (7), Em^{LEM}, was subcloned into a modified pET-32a vector (12) to form a thioredoxin fusion protein with a His_6 tag and expressed in *Escherichia coli* strain BL21(DE3) (Novagen, La Jolla, CA). The construct was verified by DNA sequencing. *E. coli* transformed with the Em^{LEM} vector was grown on either Luria Bertini or minimal medium (with $^{15}NH_4Cl$ and $^{13}C_6$-glucose as the nitrogen and carbon sources, respectively), induced with 1 mM isopropyl D-thiogalactopyranoside at A_{600} ~ 0.8, and harvested by centrifugation 3 h following induction. After harvesting, the cell pellet was resuspended in 50 ml (per liter of culture) of 50 mM Tris, pH 7.4, 100 mM NaCl, 10 mM imidazole, and 1 mM phenylmethylsulfonyl fluoride. The suspension was lysed by three passages through a microfluidizer and centrifuged at 10,000 × *g* for 20 min. The supernatant fraction was loaded onto a HisTrap HP column (5 ml; Amersham Biosciences), and the fusion protein was eluted with a 100-ml gradient of imidazole (25–500 mM). The fusion protein was then dialyzed against 20 mM Tris, pH 8.0, and 200 mM NaCl, and digested with thrombin (10 NIH units/mg of protein). Thrombin was removed by passage over a benzami-

* This work was supported by grants from the Intramural Research Program of the NIDDK, National Institutes of Health and by the AIDS Targeted Antiviral Program of the Office of the Director of the National Institutes of Health (to G. M. C. and R. C.). The costs of publication of this article were defrayed in part by the payment of page charges. This article must therefore be hereby marked "*advertisement*" in accordance with 18 U.S.C. Section 1734 solely to indicate this fact.

The atomic coordinates and experimental NMR restraints (accession codes 2ODC for free Em^{LEM} and 2ODG for the BAF_2-Em^{LEM} complex) have been deposited in the Protein Data Bank, Research Collaboratory for Structural Bioinformatics, Rutgers University, New Brunswick, NJ (http://www.rcsb.org/).

[1] To whom correspondence should be addressed: Bldg. 5, NIDKK, National Institutes of Health, Bethesda, MD 20892-0520. Tel.: 301-496-0788; Fax: 301-496-0825; E-mail: mariusc@intra.niddk.nih.gov.

[2] The abbreviations used are: BAF, barrier-to-autointegration factor; NOE, nuclear Overhauser effect; RDC, residual dipolar coupling; HSQC, heteronuclear single quantum coherence; ITC, isothermal titration calorimetry; r.m.s., root mean square.

dine-Sepharose column (1 ml; Amersham Biosciences), followed by the addition of 1 mM phenylmethylsulfonyl fluoride. The cleaved His_6-thioredoxin was removed by loading the digested proteins over a HisTrap HP column. Em^{LEM} was further purified by a Sephadex-75 gel filtration column (Amersham Biosciences) equilibrated with 50 mM potassium phosphate, pH 6.5, and 0.01% (w/v) sodium azide. This buffer was used for NMR studies on free Em^{LEM}.

Human BAF was expressed and purified as described (4). The following isotopically labeled samples were prepared: U-^{15}N/^{13}C-labeled, 10% ^{13}C-labeled and unlabeled (natural isotopic abundance) Em^{LEM}; U-^{15}N/^{13}C-labeled, U-^{15}N/^{13}C/^{2}H/[*methyl*-^{1}H]Val/Leu/Ile-labeled, 10% ^{13}C-labeled and unlabeled BAF_2 dimer. NMR samples of the BAF_2-EM^{LEM} complex were prepared in 50 mM potassium phosphate, pH 6.5, 200 mM NaCl, and 95% H_2O, 5% D_2O.

Light Scattering—Static light scattering data were obtained using an analytical Superdex-75 column (1.0 × 30 cm; GE Healthcare) with in-line multiangle light scattering (DAWN EOS, Wyatt Technology, Inc., Santa Barbara, CA) and refractive index detectors (OPTILAB DSP, Wyatt Technology Inc.). 145 μg of BAF_2 dimer mixed with or without Em^{LEM} in 125 μl of 50 mM potassium phosphate, pH 6.5, 200 mM NaCl was applied to the pre-equilibrated Superdex-75 column (1 × 30 cm; GE Healthcare) at a flow rate of 0.5 ml/min at room temperature and eluted in the same buffer.

Analytical Ultracentrifugation—Protein stocks purified in 50 mM potassium phosphate, pH 6.5, 200 mM NaCl, and 5 mM 2-mercaptoethanol were used to prepare the samples for sedimentation equilibrium experiments. Samples of the purified complex (eluted in a single peak by gel filtration chromatography) were studied at a loading concentration of 12 μM. Different stoichiometric BAF_2 dimer to Em^{LEM} mixtures were prepared at 3:1, 2:1, 1:1, 1:2, and 1:3 ratios and nominal BAF_2 concentrations of 20 μM. The 2:1, 1:1, and 1:2 mixtures were also studied at nominal BAF_2 concentrations of 13 μM. All samples were kept at 4 °C and loaded into pre-chilled cells.

Sedimentation equilibrium experiments were conducted at 4 °C on a Beckman Optima XL-A analytical ultracentrifuge. Samples of the complex and various BAF_2/Em^{LEM} mixtures were studied at rotor speeds of 16,000, 20,000, 24,000, and 28,000 rpm. Data were acquired using 6-hole cells as an average of 4 absorbance measurements at 280 nm and a radial spacing of 0.001 cm. Sedimentation equilibrium was achieved within 48 h. Data collected at different speeds and different loading concentrations were analyzed globally in terms of various species analysis models using SEDPHAT 4.1b (13) to obtain the buoyant molecular mass $M(1 - \nu\rho)$. A solution density ρ of 1.01310 cm^3/g was measured at 20 °C on a Mettler-Toledo DE51 density meter and corrected to a value of 1.0149 cm^3/g at 4 °C, which is the value used experimentally. Partial specific volumes (ν) for BAF and Em^{LEM} (at 4 °C) were calculated based on the amino acid composition using SEDNTERP: the values are 0.7287 and 0.7184 cm^3/g, respectively.

Isothermal Titration Calorimetry—ITC was performed using a high-precision VP-ITC calorimetry system (Microcal Inc.). BAF_2 dimer and Em^{LEM} were dialyzed against degassed 25 mM Tris-HCl buffer, pH 6.5, and 0.2 M NaCl prior to the experiment. BAF_2 dimer (31 μM) in the calorimetric cell at 30 °C was titrated with Em^{LEM} (at a concentration of 854 μM in the injection syringe). Analysis of the data were performed using the Origin software provided with the instrument.

NMR Spectroscopy—Spectra were recorded at 30 °C on Bruker DMX500, DRX600, DRX750, and DRX800 spectrometers. Spectra were processed using the program NMRPipe (15), and analyzed using the programs PIPP, CAPP, and STAPP (16). Sequential assignment of ^{1}H, ^{15}N, and ^{13}C resonances was achieved by means of through-bond heteronuclear scalar correlations along the protein backbone and side chains (17, 18) using three-dimensional HNCOCACB, HNCACB, (H)C(CO)NH TOCSY, H(CCO)NH-TOCSY, and CCH-COSY experiments. Interproton distance restraints were derived from three-dimensional ^{15}N- and ^{13}C-separated NOE experiments. Stereospecific assignments of valine and leucine methyl groups were obtained from a ^{1}H-^{13}C HSQC correlation spectrum recorded on 10% ^{13}C-labeled protein (19). Side chain rotamers were derived from $^{3}J_{NC'}$(aromatic, methyl, and methylene) and $^{3}J_{CC}$ (aromatic, methyl, and methylene) scalar couplings measured by quantitative *J* correlation spectroscopy (20), in combination with data from a short mixing time (40 ms) three-dimensional ^{13}C-separated NOE spectrum recorded in H_2O (21). Intermolecular interproton distance restraints were derived from three-dimensional ^{12}C-filtered/^{13}C-separated NOE experiments recorded on complexes comprising either U-^{15}N/^{13}C or U-^{15}N/^{13}C/^{2}H/[*methyl*-^{1}H]Val/Leu/Ile BAF_2 dimer complexed to unlabeled Em^{LEM}, or U-^{15}N/^{13}C-labeled Em^{LEM} complexed to unlabeled BAF_2 dimer. Residual dipolar couplings (RDCs) were measured by taking the difference in *J* couplings between aligned (~15 and ~11 mg/ml phage pf1 (22) for free Em^{LEM} and the BAF_2-EM^{LEM} complex, respectively) and isotropic media using well established procedures (23). For free Em^{LEM}, $^{1}D_{NH}$, $^{1}D_{NC'}$, and $^{2}D_{HNC'}$ RDCs were obtained. For the BAF_2-Em^{LEM} complex $^{1}D_{NH}$ RDCs were measured on complexes of ^{15}N/^{13}C-labeled BAF_2 dimer and unlabeled Em^{LEM}, and ^{15}N/^{13}C-labeled Em^{LEM} and unlabeled BAF_2 dimer (note only $^{1}D_{NH}$ RDCs are required for the structure determination of the complex because the backbones of the two proteins are treated as rigid bodies, see below; Ref. 24). The magnitudes of the axial (D_a^{NH}) and rhombic (η) components of the alignment tensor for free Em^{LEM} were obtained from a histogram of the distribution of the normalized RDCs (25). For the complex, D_a^{NH} and η were obtained by singular value decomposition using the coordinates of the free proteins (23).

Z-exchange spectroscopy was carried out using the pulse sequence described previously (26, 27) using U-^{15}N/^{13}C/^{2}H/[*methyl*-^{1}H]Val/Leu/Ile-labeled BAF_2 in the presence of 2, 3, and 4 eq of unlabeled Em^{LEM}. The auto- and exchange-peak intensities as a function of mixing time were fitted by numerically integrating the appropriate McConnell (28) differential equations and optimizing the unknown parameters (dissociation rate constant, spin-lattice relaxation rate, and scale factors) using the program FACSIMILE (29), as described previously (27, 30).

Structure Calculations—Interproton distance restraints were derived from the NOE spectra and classified into generous approximate distance ranges corresponding to strong, medium, weak, and very weak NOE cross-peak intensities (21).

Nonstereospecifically assigned methyl, methylene, and aromatic protons and ambiguous intermolecular NOEs were represented by a $(\Sigma r^{-6})^{-1/6}$ sum (31). ϕ/ψ torsion angle restraints for free Em^{LEM} were derived from backbone (N, C′, Cα, Cβ, Hα) chemical shifts using the program TALOS (32). Side chain χ torsion angle restraints were derived from ^3J heteronuclear couplings and short mixing time NOE experiments using standard procedures (21). The minimum range for the torsion angle restraints was ±20°.

All structure calculations were carried out using Xplor-NIH (33, 34) and the IVM (35) module for torsion angle and rigid body dynamics. The structure of the free Em^{LEM} domain was calculated by simulated annealing in torsion angle space (35). The structure determination of the BAF_2-Em^{LEM} complex was carried out using conjoined rigid body/torsion angle dynamics (24, 35). The target function for simulated annealing comprises: square-well potentials for interproton distance and torsion angle restraints (36), harmonic potentials for $^{13}C\alpha/^{13}C\beta$ chemical shift restraints (37), RDC restraints (38), and covalent geometry; and a quartic van der Waals repulsion potential (39), a multidimensional torsion angle data base potential of mean force (40), a backbone hydrogen bonding data base potential of mean force (41), and a radius of gyration term (42) to represent the non-bonded contacts. The radius of gyration term represents a weak overall packing potential and the target value is given by $2.2N^{0.38}$, where N is the overall number of residues (42).

Structures were displayed using the VMD-XPLOR software (43). Reweighted atomic probability density maps used to represent the conformational space sampled by the interfacial side chains within the complex were calculated and displayed as described previously (44).

RESULTS AND DISCUSSION

Structure Determination of the Free Em^{LEM} Domain—The structure of the free Em^{LEM} domain was determined on the basis of 820 experimental NMR restraints, including 110 backbone RDCs. A summary of the structural statistics is provided in Table 1, a stereoview of the superposition of the ensemble of 180 simulated annealing structures is shown in Fig. 1*A*, and a ribbon diagram is provided in Fig. 1*B*. The structure comprises a 3–10 helix (residues 2–6) and two α-helices (residues 9–19 and 28–46) oriented at an angle of 43° to one another. The structure of Em^{LEM} is very similar to our previously published structure of the BAF binding LEM domain of LAP2 (9) with a Cα atomic r.m.s. difference of 1.3 Å for 44 atoms (residues 2–46 of Em^{LEM} and 111–154 of LAP2; percentage sequence identity of 36%). The Cα atomic r.m.s. difference between the current Em^{LEM} structure and the NMR structure previously published by Wolff *et al.* (8) is 2.4 Å for residues 2–46 and 1.5 Å for residues 3–44. Although the fold and topology of the two Em^{LEM} structures are obviously the same, there are clearly differences in detail, which are significant when one wants to use the coordinates of the free Em^{LEM} domain to solve the structure of the BAF_2-EM^{Lem} complex using conjoined rigid body/torsion angle dynamics. In this regard, we note that the agreement of the Em^{LEM} coordinates of Wolff *et al.* (8) with the $^1D_{NH}$ RDCs measured for Em^{LEM} both free and bound to the BAF_2 dimer is rather poor with RDC *R*-factors (46) of 49 and 61%, respectively, determined by singular value decomposition. In contrast, the present structure of the Em^{LEM} domains agrees extremely well with the $^1D_{NH}$ RDCs measured on the BAF_2-Em^{LEM} complex with an RDC *R*-factor of 14.8%. The latter value is comparable with the value one would expect for a 1.5–2-Å resolution crystal structure (23, 47, 48) (Note that the overall orientation of the alignment tensors of free Em^{LEM} and the BAF_2-EM^{LEM} complex differ by 128°; hence the RDCs measured for Em^{LEM} in the BAF_2-Em^{LEM} complex provide a good cross-validation measure of the quality of the coordinates of free Em^{LEM}.)

TABLE 1
Structural statistics for free Em^{LEM}

⟨SA⟩ are the final 180 simulated annealing structures. $(SA)_r$ is the restrained regularized mean structure derived from the mean coordinates obtained by averaging the coordinates of the 180 simulated annealing structures best-fitted to each other. The number of terms for the various experimental restraints is given in parentheses. None of the structures exhibit interproton distance violations >0.3 Å or torsion angle violations >5°.

	⟨SA⟩	$(SA)_r$
R.m.s. deviation from experimental restraints		
Distances (Å) (489)[a]	0.016 ± 0.002	0.016
Torsion angles (°) (129)[b]	0.322 ± 0.123	0.266
$^{13}C\alpha$ shifts (ppm) (47)	1.31 ± 0.03	1.27
$^{13}C\beta$ shifts (ppm) (45)	0.72 ± 0.01	0.70
RDC *R*-factors (%)[c]		
$^1D_{NH}$ (38)	2.3 ± 0.6	3.0
$^1D_{NC'}$ (36)	14.1 ± 0.8	11.5
$^2D_{HNC'}$ (36)	14.1 ± 0.4	12.8
R.m.s. deviations from idealized covalent geometry		
Bonds (Å)	0.003 ± 0.0002	0.004
Angles (°)	0.392 ± 0.026	0.524
Impropers (°)	0.577 ± 0.080	0.618
Measures of structure quality[d]		
% Residues in most favored region		
Ramachandran plot	99.5 ± 1.1	97.6
Bad contacts per 100 residues	7.4 ± 1.8	6.4
Precision of atomic coordinates (Å)[e]		
Backbone (N, Cα, C′, O)	0.20 ± 0.06	
All heavy atoms	0.87 ± 0.09	

[a] There are 460 interproton distance restraints comprising 9 intra-residue restraints, and $160 < |i-j| = 1$ sequential, $189 < 1\,|i-j| \leq 5$ medium range and $102\,|i-j| > 5$ long range inter-residue restraints. In addition there are 58 distance restraints for 29 backbone hydrogen bonds that were added during the final stages of refinement.

[b] The torsion angle restraints comprise 46 ϕ, 45 ψ, 32 χ_1, and 6 χ_2 angles.

[c] The RDC *R*-factor, which scales between 0 and 100%, is defined as the ratio of the r.m.s. deviation between observed and calculated values to the expected r.m.s. deviation if the vectors were randomly distributed, given by $[2D_a^2(4+3\eta^2)/5]^{1/2}$, where D_a is the magnitude of the principal component of the alignment tensor and η the rhombicity (46). The value of D_a^{NH} and η, derived from the distribution of normalized RDCs (25), are 13.2 Hz and 0.60 Hz, respectively.

[d] Calculated with the program PROCHECK (45). The dihedral angle G factors for ϕ/ψ, χ_1/χ_2, χ_1, and χ_3/χ_4 are 0.64 ± 0.04, 0.39 ± 0.12, 0.21 ± 0.15, and 0.10 ± 0.21, respectively. The WHATIF second generation packing score is 1.83; a value greater than 0 is considered to represent a high quality structure (14).

[e] The precision of the coordinates is defined as the average atomic r.m.s. difference between the individual 180 simulated annealing structures and the corresponding mean coordinates best-fitted to the backbone atoms of residues 2–46. (Residues 1 and 47 at the N and C termini, respectively, are disordered.)

Stoichiometry of the BAF_2-EM^{LEM} Complex by NMR—The BAF_2-Em^{LEM} complex is in slow exchange on the chemical shift scale and portions of the ^1H-^{15}N HSQC spectra recorded as a function of various ratios of Em^{LEM} to BAF_2 dimer are shown in Fig. 2*A*. The binding of Em^{LEM} to the BAF_2 dimer disrupts the symmetry of the dimer such that the chemical shifts of many equivalent residues of the two subunits (about 55% of the ^1H-^{15}N cross-peaks for BAF) are no longer identical in the com-

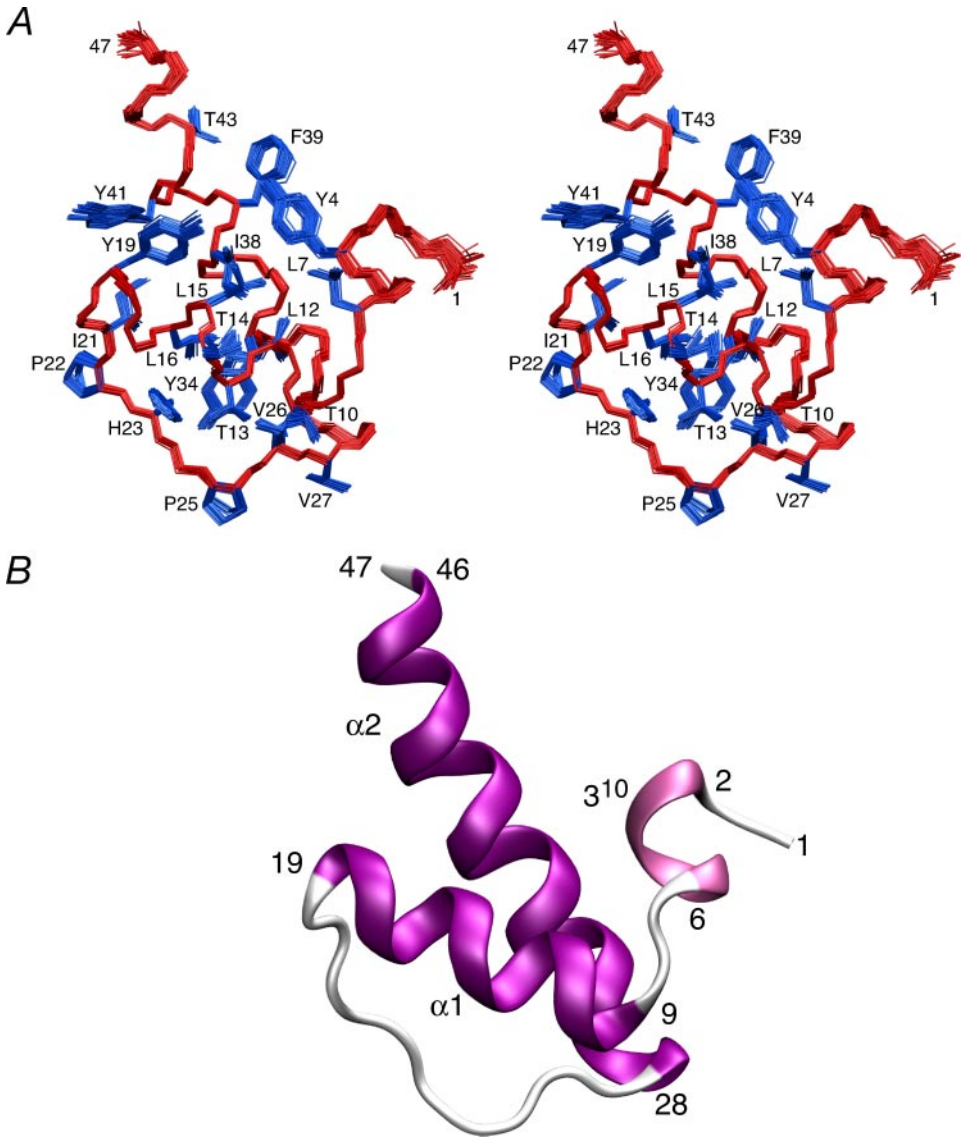

FIGURE 1. **Structure of the Em^{LEM} domain.** *A*, superposition of 180 simulated annealing structures with the backbone (N, Cα, C′) atoms in *red*, and selected side chains in *blue*. *B*, ribbon diagram of the Em^{LEM} domain with the 3–10 helix and two α-helices indicated in *different shades* of *purple*.

plex. Under the conditions of the NMR experiment (concentration of BAF_2 dimer of ~130 μM), binding of Em^{LEM} is stoichiometric with one molecule of Em^{LEM} bound per BAF_2 dimer (Fig. 2*B*). Increasing the ratio of Em^{LEM} to BAF_2 dimer above 1:1 results in no change in the intensity of the bound BAF_2 cross-peaks (Fig. 2, *A* and *B*).

Because a single molecule of Em^{LEM} binds to the BAF_2 dimer, the chemical environments of the two subunits of BAF_2 are necessarily no longer identical. The backbone of the two subunits of BAF_2, however, remains identical within coordinate errors as judged from RDC measurements (*i.e.* the values of the $^1D_{NH}$ RDCs for the two subunits of BAF_2 are identical in the complex). It should also be noted that if two molecules of Em^{LEM} bound the BAF_2 dimer symmetrically, the chemical environment and hence the chemical shifts of the two subunits of BAF_2 would be identical in the complex.

Stoichiometry of the BAF_2-EM^{LEM} Complex by Light Scattering—The calculated molecular mass of the BAF_2 dimer and the EM^{LEM} domains are 20,116 and 5,572 Da, respectively. The BAF_2 dimer elutes as a single peak with a molecular mass of 21.3 ± 0.2 kDa determined from light scattering and the refractive index data (Fig. 3*A*). A 1:1 mixture of BAF_2 dimer and Em^{LEM} results in a shift of the BAF_2 peak to a lower retention volume with a molecular mass of 25.9 ± 0.2 kDa (Fig. 3*B*). Increasing the ratio of Em^{LEM} to BAF_2 does not change the position of the latter peak and the molecular mass obtained at a ratio of BAF_2 dimer to Em^{LEM} of 1:2, 1:3, and 1:4 is 24.7 ± 0.2, 24.8 ± 0.2, and 27.4 ± 0.2 kDa, respectively. The peak eluting at ~15.4 ml with a molecular mass of 6.48 ± 0.02, 6.45 ± 0.01, and 6.76 ± 0.01 kDa shown in Fig. 3, *C-E*, respectively, corresponds to free Em^{LEM}. These results clearly indicate that the BAF_2-Em^{LEM} complex comprises one BAF_2 dimer and one molecule of Em^{LEM}. The concentration of complex upon elution is ~12 μM. The observation that the position of the peak corresponding to the complex does not change upon increasing concentration of Em^{LEM} indicates that the equilibrium dissociation constant for the complex is ≤1 μM.

Stoichiometry of the BAF_2-EM^{LEM} Complex by Analytical Ultracentrifugation—Sedimentation equilibrium experiments on the BAF_2-Em^{LEM} complex purified by size-exclusion gel filtration chromatography were carried out at rotor speeds of 16,000 to 28,000 rpm and analyzed in terms of a single ideal solute. Excellent data fits were obtained (Fig. 4) returning a molecular mass of 26.8 ± 0.4 kDa. Based on the amino acid sequence and solution density, the BAF_2 dimer and Em^{LEM} monomer have calculated molecular masses of 20,116 and 5,572 Da, respectively, indicating that the complex has a 2:1 BAF:Em^{LEM} stoichiometry (n = 1.04 ± 0.02): that is one molecule of Em^{LEM} for two subunits of BAF monomer. To confirm the stoichiometry of the complex, sedimentation equilibrium experiments were carried out on a 1:1 loading mixture of BAF_2 dimer and Em^{LEM} at concentrations of 13 and 20 μM BAF_2 dimer. A global data analysis in terms of a single ideal solute returned excellent fits with an experimental molecular mass of 25.8 ± 0.3 kDa (Fig. 4), confirming the formation of a 2:1 BAF:Em^{LEM} complex (n = 1.00 ± 0.01).

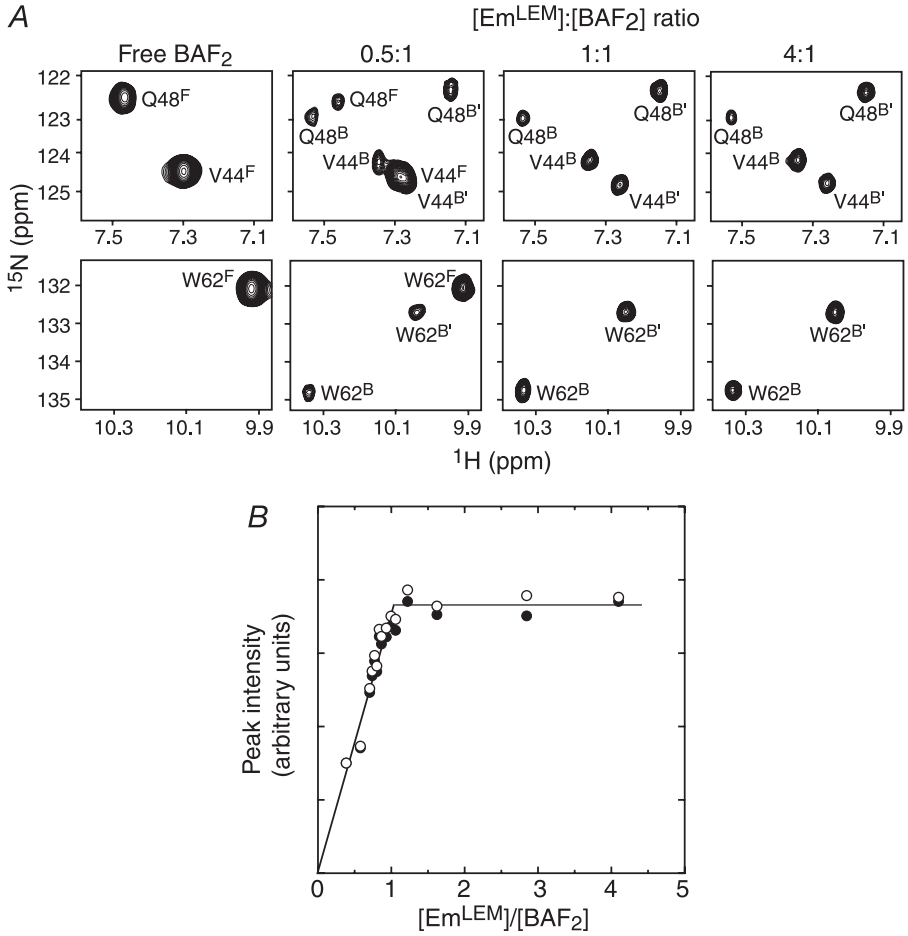

FIGURE 2. **NMR titration of Em^{LEM} and BAF_2.** *A*, portions of the ^1H-^{15}N HSQC spectra of $^{15}N/^{13}C$-labeled BAF_2 dimer (~130 μM) free and in the presence of 0.5, 1, and 4 eq of Em^{LEM}. Cross-peaks of free BAF_2 are labeled with the superscript *F*; cross-peaks for the two subunits of bound BAF_2 that are no longer chemically equivalent because of breaking of symmetry from the presence of Em^{LEM} are labeled with the superscripts *B* and *B'*. *B*, ^1H-^{15}N cross-peak intensity for the Nε-Hε group of Trp^{62} (*closed* and *open circles* correspond to the peaks labeled with the superscripts *B* and *B'*, respectively, in the *lower panels* of *A*.

Sedimentation equilibrium experiments carried out in the presence of excess Em^{LEM}, namely 1:2 and 1:3 BAF_2 dimer to Em^{LEM} mixtures, could not be modeled adequately in terms of a single ideal solute. Accordingly, data were analyzed in terms of two ideal solutes, of which one represents the free Em^{LEM} domain. Fixing the molecular mass of the smaller species to 5,572 Da, a 1:2 BAF_2 dimer to Em^{LEM} mixture returns a molecular mass of 27.0 ± 0.95 kDa for the second species with excellent data fits (data not shown). These data are consistent with the sole formation of a 2:1 BAF-Em^{LEM} complex (n = 1.05 ± 0.04). A 1:3 BAF_2 dimer to Em^{LEM} mixture containing 18.4 μM BAF_2 dimer and 55.2 μM Em^{LEM} returns a molecular mass of 29.2 ± 1.5 kDa (n = 1.14 ± 0.06) (data not shown). Thus the stoichiometry of the BAF_2-Em^{LEM} complex, comprising one molecule of Em^{LEM} bound per BAF_2 dimer, is unambiguously confirmed by three independent techniques covering a range of concentrations and molar ratios.

Equilibrium and Kinetic Characteristics of the BAF_2-EM^{LEM} Complex—ITC was used to determine the equilibrium and thermodynamic properties of the interaction of Em^{LEM} with the BAF_2 dimer. The experimental ITC binding curve obtained upon addition of Em^{LEM} to a 31 μM solution of BAF_2 dimer is shown in Fig. 5*A*. A best-fit to the experimental ITC data with a stoichiometry of one Em^{LEM} molecule bound per BAF_2 dimer yields an equilibrium dissociation constant (K_d) of 0.59 ± 0.03 μM, corresponding to a binding free energy (ΔG) of −8.63 ± 0.03 kcal mol^{-1}, and an enthalpy (ΔH) of −5.70 ± 0.05 kcal mol^{-1}. Thus, the interaction of Em^{LEM} with BAF_2 is entropically favored with ΔS = 9.7 cal mol^{-1} K^{-1}, where $\Delta S = (\Delta H - \Delta G)/T$, and T is the temperature in Kelvin. The increase in entropy upon complex formation arises from the hydrophobic effect (49) as a consequence of the displacement of ordered water at the binding interfaces of the two proteins, and suggests that the interaction between Em^{LEM} and BAF_2 is predominantly stabilized by hydrophobic interactions.

The kinetics of the interaction of unlabeled Em^{LEM} and U-$^{15}N/^{13}C/^2H$/[*methyl*-^1H]Val/Leu/Ile BAF_2 were studied by *z*-exchange spectroscopy (26, 27), which revealed the presence of chemical exchange cross-peaks between the two sets of shifts for the BAF_2 dimer in the BAF_2-Em^{LEM} complex (Fig. 5*B*). This arises from the fact that Em^{LEM} can bind to the BAF_2 dimer in two chemically equivalent ways related by a 180° rotation about

To show that these species only form a 2:1 BAF:Em^{LEM} complex, various BAF_2 dimer and Em^{LEM} mixtures were studied. In the presence of excess BAF_2, namely the 3:1 and 2:1 BAF_2:Em^{LEM} loading ratios, free BAF_2 dimer (molecular mass of 20,116 Da) and the 2:1 BAF:Em^{LEM} complex (molecular mass of 25,688 Da) are the only species expected. As the molecular masses are too similar to distinguish by sedimentation equilibrium, a mixture of these two species represents a so-called paucidisperse system and an analysis in terms of a single ideal solute should return a weight average molecular mass. The 3:1 BAF_2 dimer to Em^{LEM} loading mixture returns a weight average molecular mass of 22.2 ± 0.2 kDa with excellent data fits (data not shown), consistent with the formation of the 2:1 BAF-Em^{LEM} complex. Such a loading mixture is expected to return a weight average molecular mass of 22,147 Da if the 2:1 BAF-Em^{LEM} complex were formed. If the BAF-Em^{LEM} complex had a 2:2 stoichiometry (*i.e.* one Em^{LEM} molecule per BAF subunit), a weight average molecular mass of 24,334 Da would be expected. Data collected for the 2:1 BAF_2/Em^{LEM} loading mixture were also consistent with a 2:1 BAF-Em^{LEM} complex stoichiometry, within the error of the method.

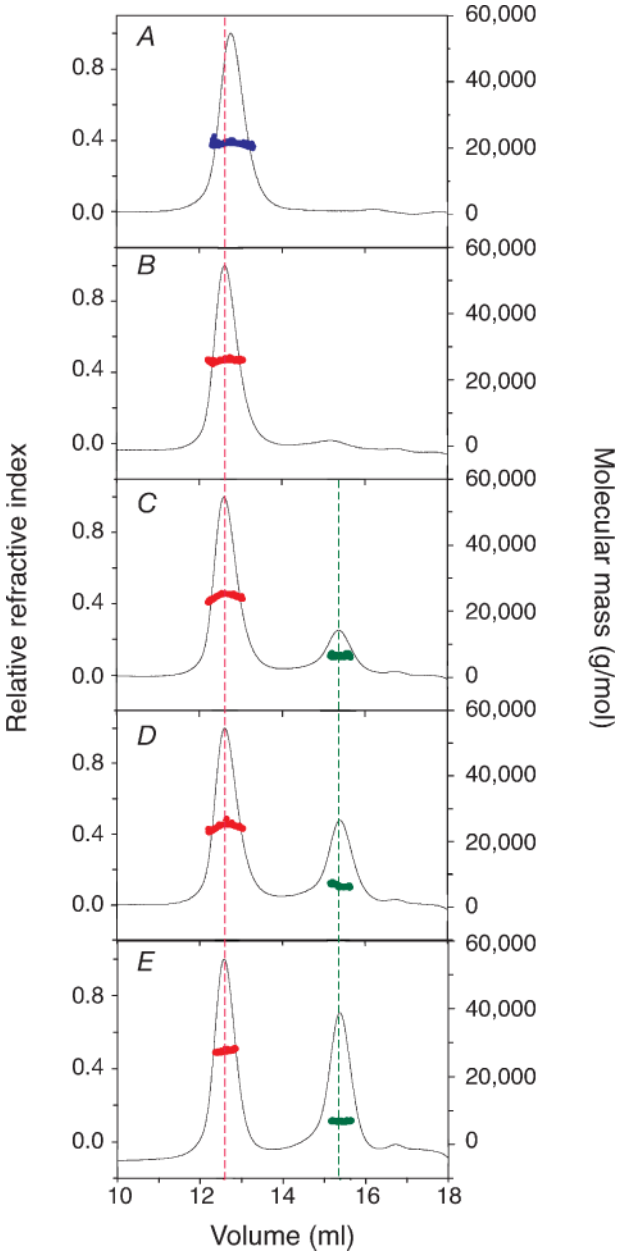

FIGURE 3. **Size exclusion chromatography and multiangle light scattering on the BAF_2-Em^{LEM} complex.** Elution profiles from an analytical S75 column (1 × 30 cm) monitored by refractive index of BAF_2 dimer alone (*A*) (145 μg in a 125-μl injection volume) and in the presence of 1 (*B*) (40 μg), 2 (*C*) (80 μg), 3 (*D*) (120 μg), and 4 (*E*) (160 μg) eq of Em^{LEM}. Assuming a ~5-fold dilution of the sample in the column, the concentration of BAF_2 and BAF_2-Em^{LEM} complex is ~12 μM upon elution. The molecular masses obtained from the light scattering and refractive index measurements correspond to a BAF_2 dimer, BAF_2 dimer-Em^{LEM} complex, and free Em^{LEM} shown in *blue*, *red*, and *green closed circles*, respectively.

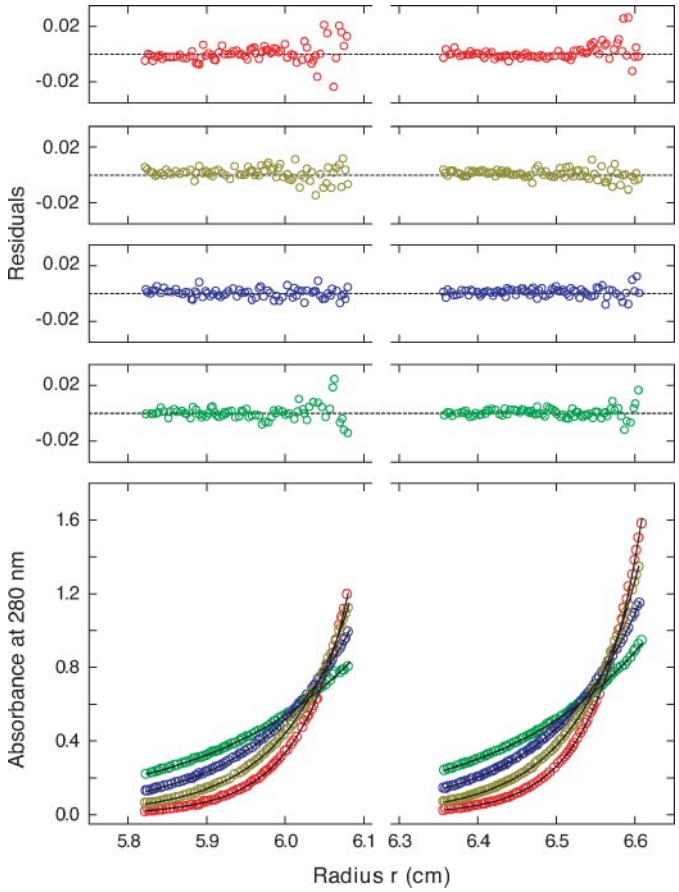

FIGURE 4. **Analytical ultracentrifugation on the BAF_2-Em^{LEM} complex.** Sedimentation equilibrium profiles obtained for the purified BAF_2-Em^{LEM} complex (*left*) and a 1:1 BAF_2/Em^{LEM} mixture (*right*) shown in terms of A_{280} *versus* the radius *r* for data collected at a loading concentration of 12 μM complex (*left*) and 13 μM BAF_2 (*right*). Data were collected at 4 °C and 16,000 (*green*), 20,000 (*blue*), 24,000 (*yellow*), and 28,000 (*red*) rpm. For clarity, alternate data points have been omitted. In both cases data were analyzed in terms of a single ideal solute to return a molecular mass consistent with that of a 2:1 BAF-Em^{LEM} complex (*i.e.* one molecule of Em^{LEM} per BAF_2 dimer). Best single ideal solute fits are shown as *black lines* through the experimental points. The corresponding distributions of the residuals are shown in the plots above. The data set shown for the 1:1 mixture was analyzed globally along with a similar sample having 20 μM BAF_2 dimer.

the C_2 symmetry axis of the BAF_2 dimer (Fig. 6). Thus cross-peaks corresponding to the two magnetically inequivalent subunits of BAF_2 in the complex are simply interchanged in the two bound states. The exchange process occurs via dissociation followed by reassociation (and note both orientations are equally probable because the two possible complexes are chemically equivalent) (Fig. 5*C*). The McConnell (28) differential equations describing the evolution of magnetization as a function of mixing time for the scheme shown in Fig. 5*C* are as follows,

$$dM_B/dt = M_F \cdot k_{on}[Em^{LEM}]_{free} - M_B(k_{off} + \rho_B) \quad \text{(Eq. 1)}$$

$$dM_{B'}/dt = M_F \cdot k_{on}[Em^{LEM}]_{free} - M_{B'}(k_{off} + \rho_B) \quad \text{(Eq. 2)}$$

$$dM_F/dt = -M_F(\rho_F + 2k_{on}[Em^{LEM}]_{free}) + k_{off}(M_B + M_{B'}) \quad \text{(Eq. 3)}$$

where M_F is the magnetization of free BAF_2, and M_B and $M_{B'}$ are the magnetizations for the two species of BAF_2 in the complex related by the 180° rotation of bound Em^{LEM}; k_{on} and k_{off} are the association and dissociation rate constants, respectively; ρ_F and ρ_B are the spin-lattice relaxation rates for BAF_2 in the free and bound states, respectively; $[Em^{LEM}]_{free}$ is the concentration of free Em^{LEM}; and $k_{on}[Em^{LEM}]_{free}$ is a pseudo-first order rate constant because the concentration of free Em^{LEM} is not perturbed during the experiment. The intensity of a given auto-peak and its associated exchange-peaks as a function of mixing time are obtained by numerical integration of Equations 1–3 with the magnetization of the species corresponding to the auto-peak set to 1 and the magnetization of the species corresponding to the exchange-peaks set to zero.

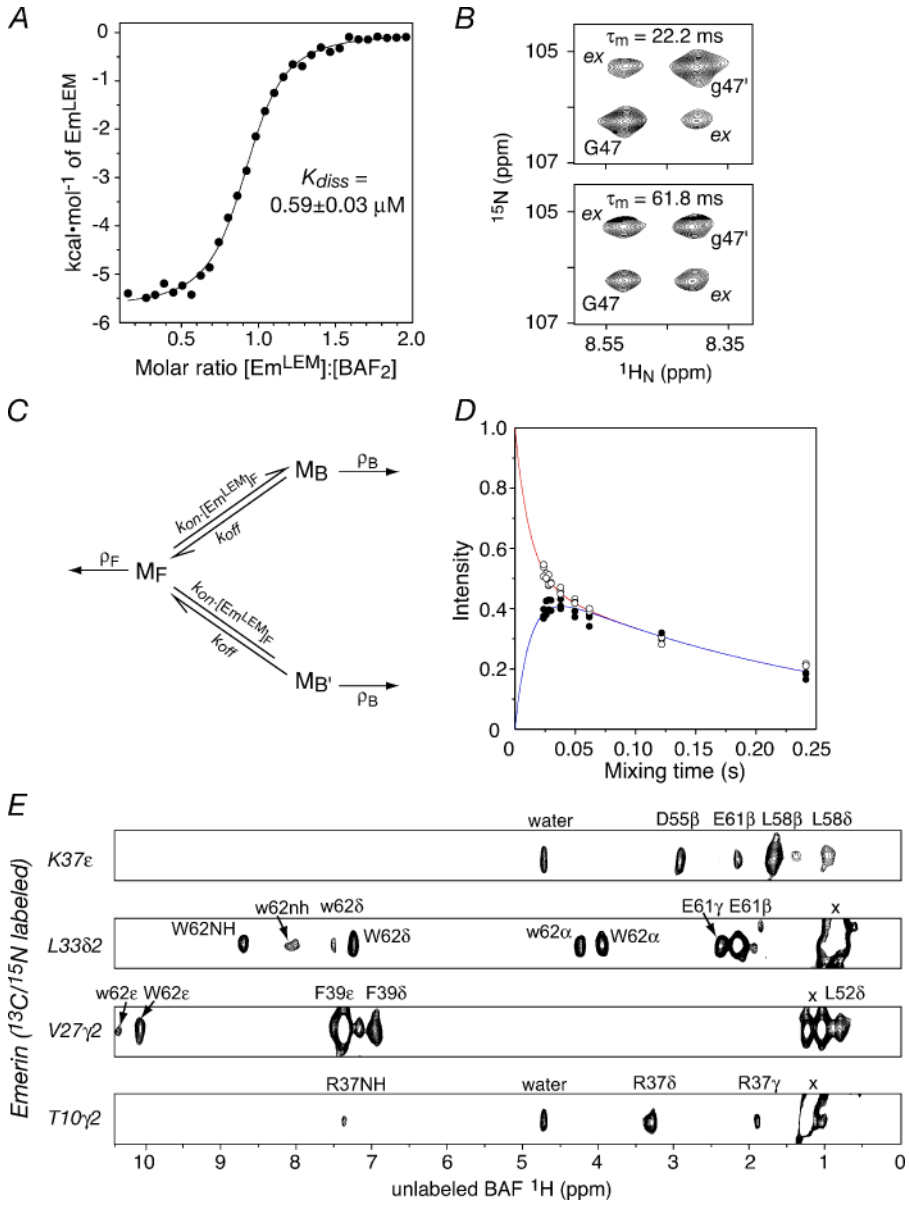

FIGURE 5. **Thermodynamics and kinetics of the BAF_2-Em^{LEM} complex.** *A*, ITC titration of BAF_2 with Em^{LEM}. The titration (3 μl per injection of 854 μM Em^{LEM}) was performed at 30 °C in a calorimetric cell (~1.8 ml) containing 31 μM BAF_2 dimer in 25 mM Tris-HCl, pH 6.5, and 0.2 M NaCl. The experimental data are shown as *solid circles*. The best-fit curve to a one site binding equilibrium is shown as a *solid line* and yields a value of $K_d = 0.59 \pm 0.03$ μM. *B*, because one molecule of Em^{LEM} binds to the BAF_2 dimer, the chemical environments of equivalent residues from the two subunits of BAF are no longer identical and display different chemical shifts, as illustrated for Gly^{47}. *Z*-exchange spectroscopy reveals the presence of exchange cross-peaks (indicated by *ex*) between equivalent residues in addition to the auto-peaks (labeled as *G47* and *g47′*). This arises from the fact that Em^{LEM} can bind to the BAF_2 dimer in two chemically equivalent ways related by a 180° rotation (see Fig. 6). *C*, kinetic scheme describing the magnetization transfer involving dissociation and reassociation of Em^{LEM} to BAF_2 in two chemically equivalent orientations. Cross-peaks corresponding to the two magnetically inequivalent subunits of BAF_2 in the complex are simply interchanged in the two bound states. M_F is the magnetization of free BAF_2; M_B and $M_{B'}$ are the magnetizations of the two bound states of BAF_2 related by the 180° rotation of Em^{LEM}; k_{on} and k_{off} are the association and dissociation rate constants, and $[Em^{LEM}]_F$ is the concentration of free Em^{LEM}; ρ_F and ρ_B are the spin-lattice relaxation rates for free and bound BAF_2 and for simplicity are considered equal because ρ_F cannot be determined from the present data. *D*, time course of the normalized auto- (*open circles*) and exchange- (*closed circles*) peaks of Gly^{47} together with the best-fit curves (*red* and *blue lines*, respectively) obtained for the kinetic model shown in *C*. The experimental data are shown at three different concentrations of free Em^{LEM} (0.39, 0.68, and 0.89 mM) with total concentrations of U-$^{15}N/^{13}C/^{2}H$/[*methyl*-^{1}H]Val/Leu/Ile-labeled of 0.42, 0.35, and 0.30 mM, respectively, and total concentration of unlabeled Em^{LEM} of 0.81, 1.03, and 1.19 mM, respectively. *E*, selected strips from a three-dimensional ^{12}C-filtered/^{13}C-separated NOE spectrum illustrating intermolecular NOEs from ^{12}C-attached protons of the BAF_2 dimer (F_1 dimension) to ^{13}C-attached protons of Em^{LEM} (F_3 dimension). The spectrum was recorded in 95% H_2O, 5% D_2O. The cross-peaks involving equivalent residues in the two subunits of BAF_2 are indicated by *upper* and *lowercase* one-letter codes.

Z-exchange experiments were carried out at three different concentrations of free Em^{LEM}, 0.39, 0.68, and 0.89 mM. The evolution of the intensities of the normalized auto- and exchange-peaks as a function of mixing time was found to be concentration independent (Fig. 5*D*). This is as expected because $k_{on}\cdot[Em^{LEM}]_{free} \gg k_{off}$, so that the apparent rate of interconversion between the magnetizations M_B and $M_{B'}$ is $k_{off}/2$ in each direction. Note also that the calculated maximum magnetization of the exchange-peak for M_F is less than 10^{-3}, and hence no exchange-peak corresponding to free BAF_2 is observed. Simultaneous best-fitting of the time courses of the intensities of the auto- and exchange-peaks (Fig. 5*D*) yields a value of $k_{off} = 78 \pm 2\ s^{-1}$. Given the value of K_d determined by ITC, the association rate constant (k_{on}) is calculated to be $\sim 1.3 \times 10^8\ M^{-1}\ s^{-1}$, typical of a diffusion-controlled protein-protein association reaction (50).

It should be noted that the exchange process observed by *z*-exchange spectroscopy is a phenomenon that can only be observed by NMR and is of no functional significance because the two binding orientations are chemically equivalent and therefore functionally identical. (It is, of course, of biophysical significance because it enables one to determine the value of the dissociation rate constant.) The existence of the exchange process does, however, have implications for the NMR structure determination of the complex. In particular, all intermolecular NOEs must be treated as ambiguous $(\Sigma r^{-6})^{-1/6}$ sums (31) because no distinction can be made *a priori* as to which BAF subunit is involved in a given intermolecular NOE. This situation is exactly analogous to the situation that pertains to the δ and ϵ protons of Phe and Tyr residues undergoing 180° ring flips. It should also be noted that because of chemical exchange between the two binding orientations (related by a 180° rotation), an NOE cross-peak from a residue of Em^{LEM} to a residue on

one subunit of BAF will be transferred by chemical exchange to the corresponding residue on the other BAF subunit. This is clearly evident in some of the strips taken from a three-dimensional ^{12}C-filtered/^{13}C-separated NOE spectrum shown in Fig. 5*E*.

Structure Determination of the BAF$_2$-Em^{LEM} Complex—The structure of the BAF$_2$-Em^{LEM} complex was solved by conjoined rigid body/torsion angle dynamics (24, 35) on the basis of 308 experimental NMR restraints including 140 backbone $^1D_{NH}$ RDCs that yield precise and accurate orientational restraints related to the relative positions of BAF$_2$ and Em^{LEM} within the complex, and 31 intermolecular interproton distance restraints derived from three-dimensional ^{12}C-filtered/^{13}C-separated NOE spectroscopy that provide translational, as well as orientational, information. In these calculations the backbone and non-interfacial side chains for the two proteins are treated as rigid bodies, whereas the interfacial side chains are given full torsional degrees of freedom (24, 35): the backbone of the BAF$_2$ dimer is held fixed, Em^{LEM} is free to rotate and translate, and the single RDC alignment tensor is free to rotate. The starting coordinates employed for the complex comprise the published NMR structure of the BAF$_2$ dimer (Protein Data Bank code 1QCK; Ref. 42) and the present NMR structure of the EM^{Lem} domain (the restrained regularized mean coordinates are used because these are the coordinates that are closest to the mean yet satisfy the experimental restraints as well as any of the individual simulated annealing structures; Ref. 51). Within the errors of the NMR coordinates there are no changes in backbone conformation upon complex formation: the $^1D_{NH}$ RDCs recorded on the complex agree with the coordinates of free BAF$_2$ dimer and Em^{LEM} with RDC *R*-factors (46) of 15.2 and 14.8%, respectively, which is comparable with values expected for 1.5–2-Å resolution crystal structures (47,

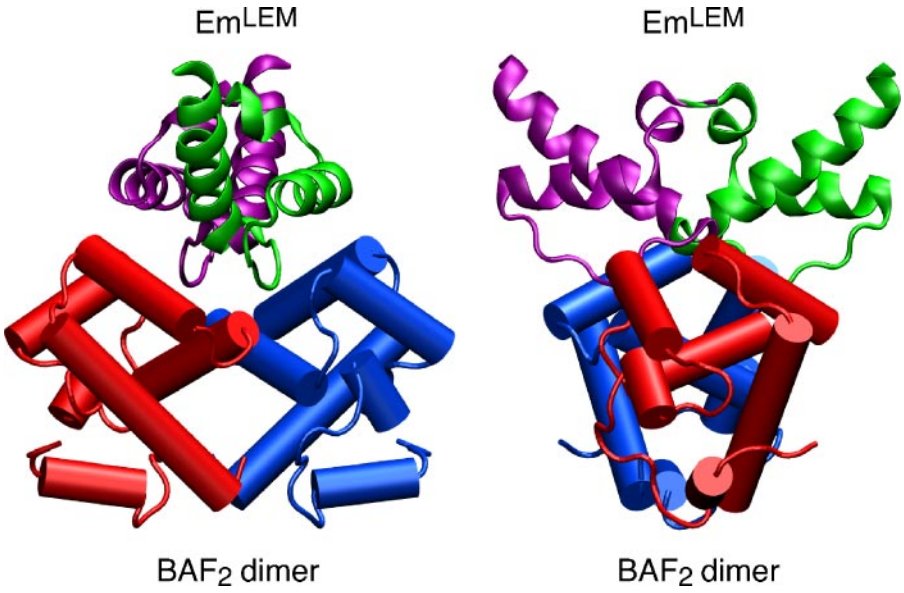

FIGURE 6. **Em^{LEM} binds to the BAF$_2$ dimer in two chemically equivalent orientations related by a 180° rotation about the C$_2$ axis of symmetry of the BAF$_2$ dimer.** The two subunits of the BAF$_2$ dimer are shown in *red* and *blue*; and the two orientations of Em^{LEM} are shown in *green* and *purple*. The structure shown represents the restrained regularized mean coordinates derived from an ensemble of 180 simulated annealing structures calculated using conjoined rigid body/torsion angle dynamics (see Fig. 7).

TABLE 2
Structural statistics for the BAF$_2$-Em^{LEM} complex
The notation is the same as that in Table 1. The number of experimental restraints for the various terms is given in parentheses.

	⟨SA⟩	(SA)$_r$
R.m.s. deviations from experimental restraints		
Interproton distances (Å) (122)[a]	0.007 ± 0.002	0.016
Side chain torsion angles (°) (46)[b]	0.033 ± 0.046	0.025
Overall RDC R-factors[c]		
$^1D_{NH}$ BAF (54 × 2)	15.3 ± 0.003	15.2
$^1D_{NH}$ Em^{LEM} (32)	14.8 ± 0.002	14.8
Measures of structure quality[d]		
Intermolecular repulsion energy (kcal mol^{-1})	3.9 ± 3.3	1.6
Intermolecular Lennard-Jones energy (kcal mol^{-1})	−14.8 ± 3.3	−4.2
Coordinate precision of the complex (Å)[e]		
Complete backbone (N, Cα, C′, O) atoms	0.13 ± 0.06	
Interfacial side chain heavy atoms	1.02 ± 0.02	

[a] The interproton distance restraints comprise 31 intermolecular interproton distances, 30 intramolecular distances related to the interfacial side chains of BAF (4 intra-residue, 9 $|i-j|=1$ sequential, 13 $1<|i-j|\leq 5$ medium range and 4 $|i-j|>5$ long range inter-residue), and 61 intramolecular distances related to the interfacial side-chains of Em^{LEM} (3 intra-residue, and 22 sequential, 29 medium range and 7 long range inter-residue).
[b] The torsion angles comprise 13 × 2 χ_1 and 4 × 2 χ_2 for the BAF$_2$ dimer, and 11 χ_1 and 1 χ_2 for Em^{LEM}.
[c] The values of D_a^{NH} and η are 10.4 and 0.5 Hz, respectively. Note that the RDR *R*-factors (46) reported in the table are obtained using a single alignment tensor for the complex. The RDC *R*-factors for BAF and Em^{LEM} obtained by singular value decomposition to the coordinates of the two proteins individually (*i.e.* with independent alignment tensors for the two proteins) are 15.2 and 14.8%, respectively, with correlation coefficients of 0.97.
[d] The intermolecular repulsion energy is given by the value of the quartic van der Waals repulsion term calculated with a force constant of 4 kcal mol^{-1} Å^{-4} and a van der Waals radius scale factor of 0.78. The intermolecular Lennard-Jones van der Waals interaction energy is calculated using the CHARMM19/20 parameters and is not included in the target function used to calculate the structures. The percentage of residues present in the most favorable region of the Ramachandran map for the NMR structure of free BAF is 89.5%.
[e] Defined as the average r.m.s. difference between the final 180 conjoined rigid body/torsion angle dynamics simulated annealing structures and the mean coordinate positions. The value quoted for the complete backbone provides only a measure of the precision with which the orientation and translation of the BAF$_2$ dimer and the Em^{LEM} domain have been determined relative to each other and does not take into account the accuracy of the NMR coordinates of free BAF$_2$ and Em^{LEM}. The excellent agreement of the RDCs measured on the complex with the coordinates of free BAF$_2$ and Em^{LEM}, however, indicates good accuracy (23, 47, 48).

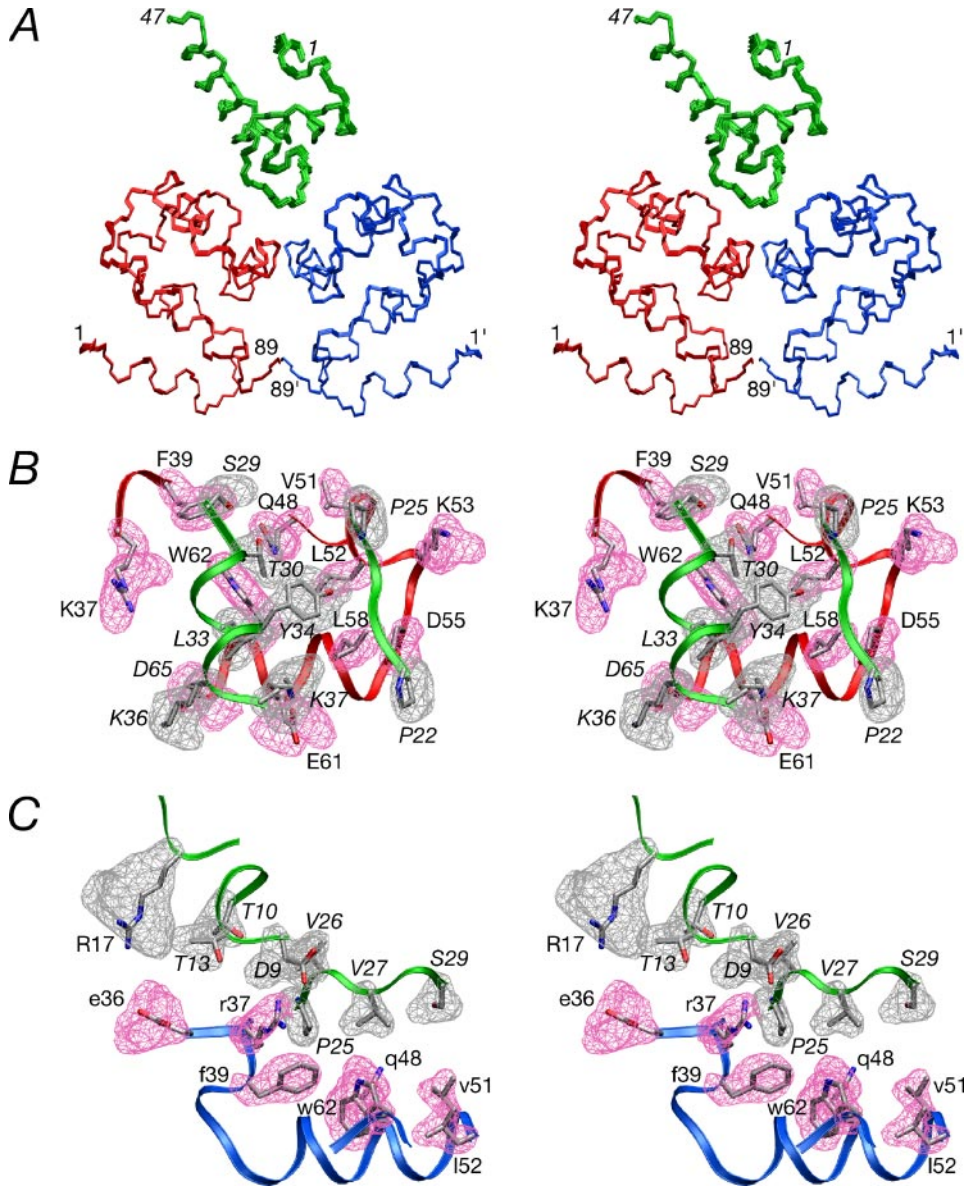

FIGURE 7. **Stereoviews of the NMR structure of the BAF_2-Em^{LEM} complex.** *A*, superposition of the backbone (N, Cα, C′) atoms) of 180 simulated annealing structures (Em^{LEM}, *green*, and the two subunits of the BAF_2 dimer shown in *red* and *blue*). Reweighted atomic probability density maps (drawn at a value of 25% maximum and calculated from the final 180 simulated annealing structures) for the interfacial side chains, illustrating the interactions between Em^{LEM} (*gray mesh*) and the *red* (*B*) and *blue* (*C*) subunits of the BAF_2 dimer (*red meshes*). The backbone (with the same color scheme as in *A*) is represented by *flat ribbons*. The side chains of the restrained regularized mean coordinates are color coded according to atom type (carbon, *gray*; oxygen, *red*; and nitrogen, *blue*).

48). The RDC *R*-factors for BAF_2 and Em^{LEM} in the refined complex (that is using a single alignment tensor for the whole complex) are the same as those obtained by singular value decomposition fitting to the coordinates of the two proteins individually. A table of structural statistics for the BAF_2-Em^{LEM} complex is provided in Table 2. A superposition of the backbone for an ensemble of 180 simulated annealing structures is shown in Fig. 7*A*, and reweighted atomic probability density maps for the interfacial side chains, derived from the ensemble, are shown in Fig. 7, *B* and *C*.

The BAF-Emerin Interface—The interaction surface between the BAF_2 dimer and Em^{LEM} is formed by a convex protrusion on Em^{LEM} comprising helix α1, the subsequent loop, and the N-terminal end of α2; and a deep concave cleft on the BAF_2 dimer comprising the C-terminal end of α2, the subsequent hairpin turn and α3 of the red subunit of BAF, and the hairpin turn between α2 and α3, the C-terminal end of α3, and the central portion of α4 of the blue subunit of BAF (Fig. 8*A*). (For clarity we distinguish the two subunits of BAF by color coding.) There is no overlap between the single Em^{LEM} binding site and the two symmetry related DNA binding sites on the BAF_2 dimer. The latter comprises the N terminus of α1, the 3–10 helix/turn/α2 motif, and the N-terminal portion of α5. 969 Å^2 of accessible surface area are buried at the interface of which 462 Å^2 originates from BAF_2 and 507 Å^2 from Em^{LEM}. The loop connecting helices α1 and α2 of Em^{LEM} interact with the red subunit of BAF, whereas α1 and the following loop interact with the blue subunit. The binding surfaces on both BAF_2 and Em^{LEM} consist of a central hydrophobic portion surrounded by a rim of polar and charged residues (Fig. 8*B*), typical of many protein-protein complexes (47). The key hydrophobic interactions involve Val^{51}, Leu^{52}, Leu^{58}, val^{51}, phe^{39}, and gly^{38} of BAF (where lowercase letters indicate residues from the blue subunit) and *Leu*^{23}, *Gly*^{24}, Phe^{25}, and *Val*^{26} of Em^{LEM} (italics denote residues of Em^{LEM}). The preponderance of hydrophobic interactions at the interface and the displacement of ordered water from these hydrophobic surfaces upon binding accounts for the positive entropic change upon complex formation observed by ITC. Key electrostatic interactions occur between Arg^{37}, Glu^{61}, and Asp^{65} of the red subunit of BAF and *Asp*^{9}, *Lys*^{38}, and *Lys*^{36}, respectively, of Em^{LEM} (Fig. 7*B*) and between glu^{36} of the blue subunit of BAF and *Arg*$_{17}$ of Em^{LEM}, and possibly the hydroxyl groups of *Thr*^{10} and *Thr*^{13} via water-mediated interactions as well (Fig. 6*C*). Additional electrostatic interactions include possible water bridged contacts between Gln^{48} of the red subunit of BAF and the hydroxyl groups of *Ser*^{29} and *Thr*^{30} of Em^{LEM} (Fig. 7*B*). Trp^{62} of the red subunit of BAF is principally involved in hydrophobic contacts with *Thr*^{30} and *Leu*^{33} (Fig. 7*B*), and trp^{62} of the blue subunit with *Val*^{27} (Fig. 7*C*). The observed interactions between BAF and Em^{LEM} are fully consistent with mutagenesis data that showed that the *G24A/P25A/V26A/V27A*, *T30A/*

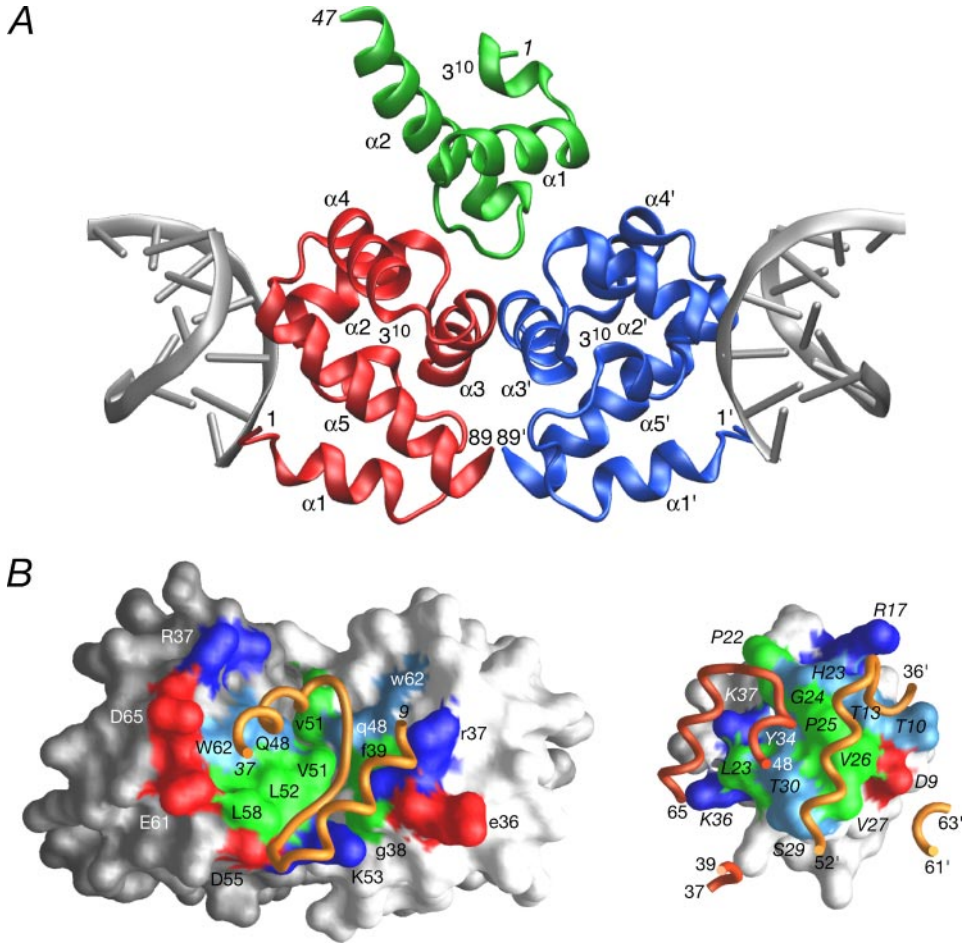

FIGURE 8. **The BAF_2-Em^{LEM} interface.** *A*, ribbon diagram of the BAF_2-Em^{LEM} complex (color coded as in Fig. 7*A*) also illustrating the position of the two DNA duplexes observed in the crystal structure of the BAF_2-DNA_2 complex (5). *B*, surface representations illustrating the binding surfaces involved in the BAF_2-Em^{LEM} complex. The binding surface on BAF_2 is shown on the *left panel* and on Em^{LEM} on the *right panel*. The binding surfaces are color coded with hydrophobic residues in *green*, polar residues in *light blue*, positively charged residues in *dark blue*, and negatively charged residues in *red*. The relevant portions of the interacting partner are shown as *gold tubes*. The surface of the non-interacting residues of the BAF_2 dimer is shown in *dark gray* for the *red subunit* and *light gray* for the *blue subunit* (as depicted in *A*). Residues of the *blue subunit* of BAF_2 are labeled in *lowercase*, and residues of Em^{LEM} in *italics*. The view in the *right-hand panel* is related to that in the *left-hand panel* by a 180° rotation about an axis parallel to the printed lines on the page.

R31A, and *Y34A/E35A/K36A/K37A* mutations significantly reduce binding of emerin to BAF (52). (Note that a fourth emerin mutation that disrupts BAF binding, *E11A/L12A* (52), does not involve the interaction surface but is predicted to destabilize the Em^{LEM} core through the introduction of a cavity as a consequence of the replacement of a leucine by the much smaller alanine side chain.)

Modulation of the Interaction of BAF with LEM Domain Proteins—The structure of the BAF_2-Em^{LEM} complex reported here, together with the structure of BAF_2 in complex with DNA (5), places constraints on how the interaction of BAF with LEM domain proteins is regulated. BAF and LEM domain proteins function as part of large nucleoprotein networks; attempts to fish out interacting partners of BAF and LEM domain proteins by biochemical techniques yields numerous proteins, most of which presumably interact indirectly.[3] LAP2 was first identified as a BAF-interacting protein in a yeast two-hybrid screen, and deletion analysis mapped a region encompassing the LEM domain to be sufficient for this interaction (53). The structure of the BAF_2-Em^{LEM} complex establishes the basis of this interaction. In *in vitro* binding studies, the LAP2 constant region has a higher affinity for BAF bound to DNA than for BAF alone and this was taken as evidence for a conformational change in BAF upon DNA binding (54). It is now clear that no conformational changes in BAF occur upon binding either DNA or the LEM domain. Alternative explanations for the higher affinity of the LAP2 constant domain for BAF bound to DNA include the possible interaction of regions outside of the LEM domain with DNA or stabilization of the complex through binding of multiple units of BAF to DNA. Modulation of the BAF-LEM interaction by regions outside the LEM domain is also suggested by the different affinities of various LAP2 isoforms for BAF (54). In addition, studies of the behavior of fluorescently labeled BAF and emerin in cells also suggest modulation of the BAF-LEM interaction (55). A direct interaction between BAF and emerin at the nuclear envelope was demonstrated by FRET analysis. However, fluorescence recovery after photobleaching experiments showed that whereas BAF was highly mobile at the nuclear envelope, emerin was much less mobile. On the basis of these results a "touch and go" model was proposed in which BAF binds emerin frequently but transiently during interphase. This association of BAF and emerin agrees nicely with the transient interaction ($k_{off} \sim 78\ s^{-1}$) we observe by NMR between BAF and the LEM domain of emerin. In contrast, BAF associates much more stably with LEM domain proteins at the "core" region of telophase chromosomes (55). This stable interaction cannot be accounted for by the interaction of BAF with the LEM domain alone, which is transient, and additional protein factors are likely involved.

Concluding Remarks—The structures of the BAF_2-Em^{LEM} and BAF_2-DNA_2 (5) complexes provides a structural basis for how BAF both bridges DNA and binds nuclear membrane proteins that contain the LEM domain. The BAF dimer is required for DNA bridging, but binding of the BAF dimer to a single LEM domain ensures that each BAF dimer

[3] R. Craigie, unpublished data.

interacts with only a single LEM-domain protein and prevents assembly of mixed complexes with multiple nuclear envelope proteins.

REFERENCES

1. Lee, M. S., and Craigie, R. (1998) *Proc. Natl. Acad. Sci. U. S. A.* **95,** 1528–1533
2. Nagano, A., Koga, R., Ogawa, M., Kurano, Y., Kawada, J., Okada, R., Hayashi, Y. K., Tsukahara, T., and Arahata, K. (1996) *Nat. Genet.* **12,** 254–259
3. Gruenbaum, Y., Margalit, A., Goldman, R. D., Shumaker, D. K., and Wilson, K. L. (2005) *Nat. Rev. Mol. Cell Biol.* **6,** 21–31
4. Cai, M., Huang, Y., Zheng, R., Wei, S. Q., Ghirlando, R., Lee, M. S., Craigie, R., Gronenborn, A. M., and Clore, G. M. (1998) *Nat. Struct. Biol.* **5,** 903–909
5. Bradley, C. M., Ronning, D. R., Ghirlando, R., Craigie, R., and Dyda, F. (2005) *Nat. Struct. Biol. Mol. Biol.* **12,** 935–936
6. Bione, S., Maestrini, E., Rivella, S., Mancini, M., Rigis, S., Romeo, G., and Toniolo, D. (1994) *Nat. Genet.* **8,** 323–327
7. Lin, F., Blake, D. L., Callebaut, L., Sjerjanc, I. S., Holmer, L., McBurney, M. W., Paulin-Levasseur, M., and Worman, H. J. (2000) *J. Biol. Chem.* **275,** 4840–4847
8. Wolff, N., Gilquin, B., Courchay, K., Callebaut, I., Worman, H. J., and Zinn-Justin, S. (2001) *FEBS Lett.* **501,** 171–176
9. Cai, M., Huang, Y., Ghirlando, R., Wilson, K. L., Craigie, R., and Clore, G. M. (2001) *EMBO J.* **20,** 4399–4407
10. Haraguchi, T., Koujin, T., Segura-Totten, M., Lee, K. K., Matsuoka, Y., Yoneda, Y., Wilson, K. L., and Hiraoka, Y. (2001) *J. Cell Sci.* **114,** 4575–4585
11. Jacque, J.-M., and Stevenson, M. (2006) *Nature* **441,** 641–645
12. Cai, M., Williams, D. C., Wang, G., Lee, B. R., Peterkofsky, A., and Clore, G. M. (2003) *J. Biol. Chem.* **278,** 25191–25206
13. Lebowitz, J., Lewis, M. S., and Schuck, P. S. (2002) *Protein Sci.* **11,** 2067–2079
14. Vriend, G., and Sander C. (1993) *J. Appl. Crystallogr.* **26,** 47–60
15. Delaglio, F., Grzesiek, S., Vuister, G. W., Zhu, G., Pfeifer, J., and Bax, A. (1995) *J. Biomol. NMR* **6,** 277–293
16. Garrett, D. S., Powers, R., Gronenborn, A. M., and Clore, G. M. (1991) *J. Magn. Reson.* **94,** 214–220
17. Clore, G. M., and Gronenborn, A. M. (1991) *Annu. Rev. Biophys. Biophys. Chem.* **20,** 29–63
18. Bax, A., and Grzesiek, S. (1993) *Acc. Chem. Res.* **26,** 131–138
19. Neri, D., Szyperski, T., Otting, G., Senn, H., and Wüthrich, K. (1989) *Biochemistry* **28,** 7510–7516
20. Bax, A., Vuister, G. W., Grzesiek, S., Delaglio, F., Wang, A. C., Tschudin, R., and Zhu, G. (1994) *Methods Enzymol.* **239,** 79–106
21. Clore, G. M., and Gronenborn, A. M. (1998) *Trends Biotechnol.* **16,** 22–34
22. Clore, G. M., Starich, M. R., and Gronenborn, A. M. (1998) *J. Am. Chem. Soc.* **120,** 10571–10572
23. Bax, A., Kontaxis, G., and Tjandra, N. (2001) *Methods Enzymol.* **339,** 127–174
24. Clore, G. M. (2000) *Proc. Natl. Acad. Sci. U. S. A.* **97,** 9021–9025
25. Clore, G. M., Gronenborn, A. M., and Bax, A. (1998) *J. Magn. Reson.* **133,** 216–221
26. Farrow, N. A., Zhang, O., Forman-Kay, J. D., and Kay, L. E. (1994) *J. Biomol. NMR* **4,** 727–734
27. Iwahara, J., and Clore, G. M. (2006) *J. Am. Chem. Soc.* **128,** 404–405
28. McConnell, H. M. (1958) *J. Chem. Phys.* **28,** 430–431
29. Chance, E. M., Curtis, A. R., Jones, I. P., and Kirby, C. R. (1979) *FACSIMILE: A Computer Program for Flow and Chemistry Simulation and General Initial Value Problems*, Atomic Energy Research Establishment Report R8775, Harwell, H. M. Stationary Office, London
30. Clore, G. M., Omichinski, J. G., and Gronenborn, A. M. (1991) *J. Am. Chem. Soc.* **113,** 4350–4351
31. Nilges, M. (1993) *Proteins* **17,** 297–309
32. Cornilescu, G., Delaglio, F., and Bax, A. (1999) *J. Biomol. NMR* **13,** 289–302
33. Schwieters, C. D., Kuszewski, J., Tjandra, N., and Clore, G. M. (2003) *J. Magn. Reson.* **160,** 66–74
34. Schwieters, C. D., Kuszewski, J., and Clore, G. M. (2006) *Prog. Nucl. Magn. Reson. Spec.* **48,** 47–62
35. Schwieters, C. D., and Clore, G. M. (2001) *J. Magn. Reson.* **152,** 288–302
36. Clore, G. M., Nilges, M., Sukuraman, D. K., Brünger, A. T., Karplus, M., and Gronenborn, A. M. (1986) *EMBO J.* **5,** 2729–2735
37. Kuszewski, J., Gronenborn, A. M., and Clore, G. M. (1995) *J. Magn. Reson. Ser. B* **106,** 92–96
38. Clore, G. M., Gronenborn, A. M., and Tjandra, N. (1998) *J. Magn. Reson.* **31,** 159–162
39. Nilges, M., Gronenborn, A. M., Brünger, A. T., and Clore, G. M. (1988) *Protein Eng.* **2,** 27–38
40. Clore, G. M., and Kuszewski, J. (2002) *J. Am. Chem. Soc.* **124,** 2866–2867
41. Grishaev, A., and Bax, A. (2004) *J. Am. Chem. Soc.* **126,** 7281–7292
42. Kuszewski, J., Gronenborn, A. M., and Clore, G. M. (1999) *J. Am. Chem. Soc.* **121,** 2337–2338
43. Schwieters, C. D., and Clore, G. M. (2001) *J. Magn. Reson.* **149,** 239–244
44. Schwieters, C. D., and Clore, G. M. (2002) *J. Biomol. NMR* **23,** 221–225
45. Laskowski, R. A., MacArthur, M. W., Moss, D. S., and Thornton, J. M. (1993) *J. Appl. Crystallogr.* **26,** 283–291
46. Clore, G. M., and Garrett, D. S. (1999) *J. Am. Chem. Soc.* **121,** 9008–9012
47. Williams, D. C., Cai, M., and Clore, G. M. (2004) *J. Biol. Chem.* **279,** 1449–1457
48. Williams, D. C., Lee, J. Y., Cai, M., Bewley, C. A., and Clore, G. M. (2005) *J. Biol. Chem.* **280,** 29269–29276
49. Dill, K. A. (1990) *Biochemistry* **31,** 7134–7155
50. Fersht, A. R. (1999) *Structure and Mechanism in Protein Science*, W. H. Freeman Co., New York
51. Clore, G. M., and Gronenborn, A. M. (1998) *Proc. Natl. Acad. Sci. U. S. A.* **95,** 5891–5898
52. Lee, K. K., Haraguchi, T., Lee, R. S., Koujin, T., Hiraoka, Y., and Wilson, K. L. (2001) *J. Cell Sci.* **114,** 4567–4573
53. Furukawa, K. (1999) *J. Cell Sci.* **112,** 2485–2492
54. Shumaker, D. K., Lee, K. K., Tanhehco, Y. C., Craigie, R., and Wilson, K. L. (2001) *EMBO J.* **20,** 1754–1764
55. Shimi, T., Koujin, T., Segura-Totten, M., Wilson, K. L., Haraguchi, T., and Hiraoka, Y. (2004) *J. Struct. Biol.* **147,** 31–41